The protein-binding pocket of Botulinum neurotoxin B accommodates a preassembled synaptotagmin / ganglioside complex

Authors

Jorge Ramirez-Franco,[1†] Fodil Azzaz,[1†] Marion Sangiardi,[1] Géraldine Ferracci,[2] Fahamoe Youssouf,[1] Michel R. Popoff,[3] Michael Seagar,[1] Christian Lévêque,[1*] Jacques Fantini,[1] Oussama EL FAR[1*]

Affiliations

[1]UMR 1072, INSERM, Unité de Neurobiologie des canaux Ioniques et de la Synapse, Aix-Marseille Université, 13015 Marseille, France.

[2]Aix-Marseille Université, CNRS, INP, Institute of Neurophysiopathology, UMR7051, PINT, PFNT, Marseille, France.

[3]Institut Pasteur, Unité des Toxines Bactériennes, UMR CNRS 2001, Paris, France.

[†]These authors contributed equally to this work

[*]Corresponding authors. Email: christian.leveque@univ-amu.fr (CL); oussama.el-far@inserm.fr (OEF)

Abstract

Botulinum neurotoxin serotype B (BoNT/B) uses two separate protein and polysialoglycolipid-binding pockets to interact with synaptotagmin 1/2 and gangliosides. However, an integrated model of BoNT/B bound to its neuronal receptors in a native membrane topology is still lacking. Using a panel of in silico and experimental approaches, we present here a new model for BoNT/B binding to neuronal membranes, in which the toxin binds to a preassembled synaptotagmin-ganglioside GT1b complex and a free ganglioside. This interaction allows a lipid-binding loop of BoNT/B to engage in a series of concomitant interactions with the glycone part of GT1b and the transmembrane domain of synaptotagmin. Furthermore, our data provide molecular support for the decrease in BoNT/B sensitivity in Felidae that harbor the natural variant synaptotagmin2-N_{59}Q. These results reveal multiple interactions of BoNT/B with gangliosides and support a novel paradigm in which a toxin recognizes a protein/ganglioside complex.

Teaser: A new molecular mechanism for botulinum neurotoxin type B binding

Short title
A new molecular mechanism for BoNT/ B binding

Introduction

Botulinum neurotoxins (BoNTs), are a family of potent protein toxins produced by anaerobic gram-positive Clostridia (*1*) (*2*). BoNTs are classified as seven different serotypes from BoNT/A to G, further divided into subtypes with different amino acid sequences, although additional BoNTs are still being discovered, including mosaic toxins derived from a combination of different serotypes (*1*) (*3*).

BoNTs are the etiological agents of botulism, a rare but severe disease affecting many vertebrates, which results from the inhibition of acetylcholine release in the peripheral nervous system, causing flaccid paralysis. At the same time, BoNT/A, and to a lesser extent BoNT/B, are widely exploited for therapeutic applications (*4*) (*5*) (*6*).

BoNTs intoxicate neurons using a multistep mechanism based on a tri-modular neurotoxin design. BoNTs are structurally similar to AB toxins with a 100 kDa heavy chain (HC) and a 50 kDa catalytic light chain, associated via a disulphide bond and non-covalent interactions. After entering the circulation, BoNTs target high affinity receptors on peripheral nerve terminals via the HC domain. The amino-terminal domain of the HC then translocates the enzymatic light chain into the cytoplasm where the latter cleaves one of the three intracellular SNARE proteins (VAMP1-3, SNAP-25 or syntaxin 1) necessary for synaptic vesicle fusion and neurotransmitter release (*5*). The BoNT carboxyl-terminal sub-domain of HC, organized into a β-trefoil fold, displays two independent binding pockets, which bind two distinct classes of receptors.

The first receptor to be discovered is a ganglioside, typically GT1b or GD1a, that is recognized by a ganglioside-binding site (GBS1), conserved in most BoNTs. Gangliosides are a family of diverse amphipathic glycosphingolipids abundantly expressed in the outer leaflet of all vertebrate cells. GM1, GD1a, GD1b and GT1b represent the vast majority (>90%) of adult mammalian brain gangliosides, composed of a ceramide, imbedded in the outer leaflet of the plasma membrane, linked to a common tetrasaccharide core with sialic acids attached to galactose residues (*7*). Gangliosides associate with cholesterol in tightly packed lipid domains that are in dynamic equilibrium with less ordered membrane regions and can support lipid and protein-lipid interactions

in *cis* and *trans* configurations (*7*) (*8*). Moreover, microdomains containing gangliosides provide an entry pathway for several viruses and other pathogens (*9*) (*10*) (*11*).

The second receptor is a protein, corresponding to the luminal sequence of a synaptic vesicle protein: synaptotagmin 1 and 2 (SYT) for BoNT/B, G and the mosaic toxin BoNT/DC or SV2 for BoNT/A, D, E, F although the identity of BoNT/D protein receptor is still to be confirmed (*2*). BoNT/C has no identified protein receptor, but like BoNT/D, harbors an additional ganglioside-binding pocket distinct from GBS1 and termed "sialic-binding site" that overlaps with the SYT-binding pocket of BoNT/B, contributing to toxicity (*12*) (*13*) .

Besides these two receptors, a solvent-exposed lipid-binding loop (LBL), present in BoNT/B, C, D, G and BoNT/DC is localized between GBS1 and the protein (BoNT/B, G and DC) or sialic acid-binding pocket (BoNT/C and BoNT/D), participates in the recognition of neuronal membranes (*2*) (*14*). This loop interacts with lipids and/or gangliosides and its deletion reduces dramatically BoNT toxicity, but it is not clear whether it can directly bind to the carbohydrate part of gangliosides (*14*) (*15*). Notably, tetanus toxin a Clostridium neurotoxin structurally related to BoNTs and sharing the highest sequence identity with BoNT/B, also has an LBL in addition to two ganglioside binding sites, like BoNT/C (*16*).

The exceptional neurotropism of BoNT/B is conferred by interaction with the extracellular juxtamembrane domain (JMD) of SYT, that is translocated to the plasma membrane by synaptic vesicle fusion. SYT1 and SYT2 have comparable biochemical properties and similar functions, regulating exo-endocytic recycling of synaptic vesicles by interacting with cytosolic proteins such as the adaptor protein AP2, as well as with specific lipids like cholesterol and PIP2 (*17*) (*18*) (*19*). While SYT1 is widely distributed in terminals of autonomic and sensory neurons, as well as in some neuromuscular junctions, SYT2 is the dominant isoform at most neuromuscular junctions (*5*). Co-crystallization data indicate that BoNT/B binds SYT1 and SYT2 in a very similar manner using a saddle-shaped pocket interacting with 10–14 SYT JMD residues (*20*) (*21*) (*22*) (*6*). The extracellular domain of SYT is not structured in solution, but the JMD of SYT adopts a helical conformation upon binding to BoNT/B (*20*) (*21*) (*22*) (*6*). In the absence of gangliosides, BoNT/B displays a much higher affinity for rat SYT2 (40 nM) than for SYT1, due to a small difference in primary sequence in the SYT JMD (*20*). Although BoNT/B has low affinity for GT1b (µM range) (*14*) (*15*), the latter drastically increases BoNT/B affinity (~0.4 nM) for membranes containing SYT (*23*) (*24*) (*25*). In detergent, the synergistic effect of GT1b requires the presence of the SYT transmembrane domain (TMD) (*26*) (*27*) and high affinity binding is only reached in reconstituted systems containing lipids as well as the transmembrane domains of SYT and GT1b, suggesting a role for the intramembrane segments in toxin binding (*22*) (*24*). As the available structural data

were obtained in the absence of apolar domains of BoNT/B receptors (*21*) (*20*) (*22*) (*6*), how BoNT/B binds to its receptors in a membrane context remains to be elucidated.

Recently we reported that the transmembrane and juxtamembrane domains of SYT interact with complex gangliosides inducing an α–helical structure (*25*). A mutation (SYT1-K_{52}A) that decreases GT1b assembly with SYT1, abolished BoNT/B binding in neuroendocrine cells, suggesting that the preassembly of a GT1b/SYT complex is crucial for BoNT/B interaction. Using a panel of in silico and experimental approaches, we now report that the SYT-binding pocket of BoNT/B can accommodate the preassembled GT1b/SYT complex and that the BoNT/B LBL interacts with the TMD of SYT and its associated GT1b molecule. We thus propose a new model for BoNT/B-SYT interaction taking into account the membrane topology of neuronal toxin receptors, a parameter that has not been considered in previous structural studies.

Results

BoNT/B binds to SYT pre-assembled with GT1b

The JMD of SYT binds GT1b (*25*) via a consensus ganglioside-interaction motif that overlaps with the described BoNT/B-SYT interaction domain (*22*). We therefore addressed the question as to whether BoNT/B can bind to a SYT/GT1b complex. To investigate this point, we developed an SPR-based approach, consisting in capturing a peptide encompassing the JMD of SYT (pSYT1 32-57 or pSYT2 40-66, fig. S1) on a sensor chip, assembling a SYT/GT1b complex and then evaluating BoNT/B binding. GT1b diluted in running buffer interacted strongly with pSYT1 or pSYT2 immobilized on a sensor chip (Fig. 1A). The interaction was specific, as no binding occurred on a control pSYT9 peptide (Fig. 1A, fig. S1). Ganglioside binding to pSYT was detected at 10 nM GT1b (fig. S2A), a concentration far below its critical micellar concentration (*28*) and was dose-dependent (fig. S2B). Estimation of the ganglioside/peptide molar ratio indicated that a mean of 3 molecules of GT1b were bound per peptide (3.04 ± 0.4, n= 7 independent experiments using pSYT1 or pSYT2). This observation is compatible with ceramide-mediated multimeric self-assembly of gangliosides that occurs in lipid rafts (*29*). The interaction of the JMD of SYT with GT1b was further corroborated using antibodies that specifically recognize the JMD of SYT. As shown in fig. S2C and D, GT1b bound to SYT, masks the recognition domain of anti-SYT JMD antibodies and inhibits their binding to SYT. Altogether, these results demonstrate that the ganglioside binding site of the JMD of SYT immobilized on a chip can stably capture GT1b. This experimental protocol mimics native conditions where SYT binds one GT1b molecule while being surrounded by other free GT1b molecules thus allowing BoNT/B to interact with SYT/GT1b and free GT1b using the SYT-binding pocket and GBS1 respectively.

We then compared BoNT/B binding to SYT and SYT/GT1b complex. In the absence of GT1b, BoNT/B binding yielded a transient SPR signal on pSYT1 (Fig. 1B first arrow), consistent with its reported low affinity (*25*) (*20*). GT1b was then immobilized on pSYT1 (Fig. 1B second arrow) before a subsequent injection of BoNT/B on the SYT/GT1b complex (Fig. 1B last arrow). Compared to pSYT1 alone, GT1b interaction with pSYT enhanced BoNT/B binding during the association phase, with a slower dissociation kinetic. This increase in BoNT/B affinity due to GT1b association with pSYT1 is similar to the effect of GT1b measured in proteoliposomes containing full length SYT1 (*25*). The potentiation of BoNT/B binding by GT1b depended on the amount of gangliosides bound to SYT, reaching a plateau (Fig. 1C, fig. S3A). To rule out the possibility that GT1b alone produces an enhancement of BoNT/B binding independently of SYT, we used a mutant SYT1 peptide ($F_{46}A$) that is unable to bind BoNT/B, but still interacts with GT1b (*21*). As shown in fig. S3A, in contrast to pSYT1/GT1b complex, BoNT/B did not interact with pSYT1-$F_{46}A$/GT1b complex in agreement with the low affinity of BoNT/B for gangliosides. BoNT/B binding does not induce GT1b dissociation from pSYT/GT1b complex, as anti-GT1b antibodies detected the same amount of GT1b before and after BoNT/B binding (fig. S3B and C). BoNT/B binding to pSYT2 was also measured when GT1b was bound to SYT2, with the difference that BoNT/B signals were higher on pSYT2 than on pSYT1 in the absence of ganglioside, in accordance with their relative affinity (Fig. 1, fig. S3D). As for SYT1, the presence of GT1b bound to SYT2, promoted BoNT/B interaction with SYT2, increasing binding affinity mainly by decreasing the dissociation rate of BoNT/B from pSYT2 (fig. S3D). Altogether, these results demonstrate that BoNT/B binds to a preassembled SYT/GT1b complex.

Molecular modeling of BoNT/B bound to a SYT/GT1b complex

In order to obtain molecular insight into the interaction of BoNT/B with SYT1-GT1b and SYT2-GT1b complexes, with specific information on the fate of the LBL upon toxin binding, we developed a molecular modeling strategy that takes into account membrane topology. Using the initial coordinates of toxin-SYT (PDB 4KBB, 6G5K and 2NP0), we constructed a full system consisting of a SYT-GT1b complex, a GD1a-toxin complex and a cholesterol molecule. After several rounds of energy minimization, a stable complex was obtained for both systems including SYT1 (Fig. 2 A) and SYT2 (Fig. 2 B). The initial conditions had to be slightly adjusted to take into account the TM domain of SYT and the ceramide part of the GD1a ganglioside which were absent from the crystal structure. These conformational constraints respected the overall geometry of the membrane, except that a gap between GD1a and the TM domain of SYT was filled by a cholesterol molecule (*17*). BoNT/B interacts with free GD1a and GT1b associated with SYT (~25 % and ~ 15

% of the total energy respectively) but in both cases the major contribution of toxin binding was due to SYT (~ 60% of the total energy) as shown in the pie chart in Fig. 2. A key feature of our models is the insertion of the LBL loop between GT1b and SYT (Fig. 2, fig. S4B). The overall energy of interaction of BoNT/B-SYT complex is around -600 kJ/mol (-592 kJ/mole for SYT1 versus -664 kJ/mole for SYT2).

BoNT/B-SYT interaction: The toxin was found to interact with a significant part of the extracellular regions of SYT1 (E_{36}-W_{58}) and SYT2 (E_{44}-W_{66}) via the SYT binding pocket, including loops Y_{1183}-K_{1188}, P_{1197}-D_{1202} and K_{1113}-P_{1117} (fig. S4A, Fig. 3). The SYT helix, pre-conformed by GT1b, extends from E_{36} to H_{51} in SYT1 and E_{44} to N_{59} in SYT2, whereas a small distortion of the helix was observed in the central part of BoNT/B-SYT interface (Fig. 2, fig. S4A). Almost all amino acids of BoNT/B that interact with SYT in the crystal structure were found in contact with SYT and/or GT1b in our models (Table S1). However, the conformational adjustment induced by the TM domain of SYT slightly turned the helix, generating a different interaction map with BoNT/B, compared to the BoNT/B-SYT binding interface determined by X-ray diffraction crystallography without membrane constraints. A detailed analysis of the contribution of amino acid residues of SYT and of the toxin revealed the evolution of the complex between the initial crystal conditions and the presented models (Table S1, Table S2). SYT1-F_{46} and SYT2-F_{54}, which initially interacted with GT1b in SYT/GT1b complexes (*25*), engage interactions with residues 1115-1117 of the toxin while retaining ganglioside association (Fig. 3, Fig. 5, fig. S5). A superposition of the crystal structure with our models is shown in Fig. 4 for SYT1-F_{46} and M_{47} and its SYT2 counterparts that are described as key energetic hotspot residues in the crystal structure. In the case of SYT1 the aromatic ring of F_{46} (white) is replaced in the model by the apolar side chain of M_{47} (Fig. 4A, light blue). Consequently, most of the amino acid residues of the toxin that were in contact with F_{46} now interact with M_{47}. In the case of SYT2 a similar substitution was evidenced between F_{54} in the crystal structure (white) and F_{55} in our model (Fig. 4B, light blue). Interestingly the aromatic ring of both residues is oriented in a similar way so that the pi-pi network involving residues Y_{1183}, F_{1194} and F_{1204} of the toxin was still operative. These models uncover several additional SYT JMD residues compared to crystal data (E_{36}, D_{37}, S_{40}, K_{41}, Q_{44}, N_{48}, H_{51} in SYT1 and E_{44}, A_{48}, K_{49}, E_{52}, N_{56}, N_{59} in SYT2) (Fig. 3, Table S2). Among them, SYT1-H_{51} and SYT2-N_{59} residues are facing the toxin and exhibit a high energy of interaction involving BoNT/B residues Y_{1183}, K_{1187}, E_{1191} and E_{1203} (Fig S6). In addition to the SYT/binding pocket, the BoNT/B LBL participates in the toxin-SYT complex by interacting tightly with apolar extramembrane (L_{50}, I_{53}, L_{55}, P_{56}) and membrane-embedded (A_{59}, A_{62}, I_{63}, V_{66}) residues of SYT1 (Fig. 3, Table S2A). Similar interactions were observed with homologous residues of SYT2 (Fig. 3, Table S2B).

SYT-GT1b interaction: GT1b imposes an angle of about 45° between the JMD of SYT and the membrane (Fig. 2). The mapping of the molecular interactions between GT1b and either SYT1 (Fig. 5 A) or SYT2 (Fig. 5 B) and the toxin revealed that the binding involved the ceramide part of GT1b and the four terminal sugars and sialic acids (Glc1 and Gal2 are not involved in binding). The overall binding energy between SYT and GT1b was conserved upon interaction with BoNT/B (Table S2). Interestingly, we noted a rearrangement involving F_{46} in SYT1 and its homologous F_{54} in SYT2 that reinforced the interaction with GT1b upon toxin binding (+32% and +90% for SYT1 and SYT2 respectively), involving Gal4, Sia5 and Sia6 (Fig. 5, Table S2, fig. S7). In contrast, SYT1-K_{52}, I_{53}, L_{55}, W_{58} and SYT2-K_{60}, I_{61}, W_{66} that were interacting initially with the Sia6 and Sia7 of GT1b in the preassembled SYT/GT1b complex, lose energy upon toxin binding (-92% and -47% respectively, Table S2, fig. S7), suggesting also a molecular rearrangement in this region.

BoNT/B-GT1b and GD1a interactions: In the minimized complexes, both the LBL and the beta hairpin loop K_{1113}-P_{1117} that interact with SYT, also bind to sialic acids of GT1b bound to SYT (Fig. 5, Table S1B, fig. S8B). The LBL binds to Sia 7 whereas the K_{1113}-P_{1117} loop binds to Sia 5 and Sia 6 (Fig. 5). Remarkably, as shown in fig. S8B, the BoNT/B loop K_{1113}-P_{1117} corresponds to conserved β-hairpin loops E_{1114}-V_{1117}, A_{1126}-R_{1129} and K_{1143}-D_{1147} of BoNT/D, BoNT/C and tetanus toxin respectively which contribute to the sialic acid binding site (*16*) (*12*) (*13*) (*30*). Our model suggests that the BoNT/B-protein binding pocket has an evolutionarily conserved ability to bind sialic acids that are brought by the SYT-associated ganglioside in the case of BoNT/B. Concerning the canonical ganglioside binding site, the BoNT/B residues interacting with the sugar part of GD1a were globally conserved after minimization compared to structural data (Table S3).

Finally, it is worth noting that, in the minimized complex, cholesterol interacts with the TM domain of SYT, occupying a space created by the addition of the ceramide part of GD1a. Cholesterol increases the stability of the complex through a set of London forces with the ceramide part of GD1a and the TMD domain of SYT (Table S4). These data raise the interesting notion that cholesterol could play an active role in the initial steps of toxin binding to lipid rafts in agreement with a previous description of SYT/cholesterol interactions (*17*).

Altogether these results suggest that BoNT/B interacts with the JMD and TMD domains of SYT along with two ganglioside molecules, one associated with SYT and the other with the ganglioside binding pocket of the toxin, with interconnection of the different intramembrane domains.

The lipid binding loop of BoNT/B binds to GT1b and SYT

Our molecular modeling data suggest that the LBL could physically interact with SYT and GT1b. In order to corroborate the accuracy of these in silico predictions, we experimentally investigated

BoNT/B LBL binding to GT1b and SYT. We used the Langmuir monolayer method and recorded surface pressure changes in GT1b or SYT2-TM monolayers induced by a water-soluble BoNT/B peptide p1242-1256 encompassing the LBL (fig. S1). Injection of p1242-1256 underneath a monolayer of GT1b yielded an increase in surface pressure (Fig. 6A), whereas limited interaction was found with lyso-LacCer (a lipid with an inverted conic shape resembling gangliosides) or sphingomyelin (a major sphingolipid component of lipid rafts). The absence of interaction with the ceramide domain of sphingomyelin indicates that the LBL of BoNT/B interacts preferentially with the sugar part of GT1b.

In order to address the interaction of BoNT/B LBL with SYT, we used a SYT2 G_{40}-S_{87} peptide encompassing its JMD and TMD (fig. S1) that was spread at the air-water interface and incubated with p1242-1256 added in the aqueous subphase. As shown in Fig. 6B, the LBL strongly bound to the SYT2-TMD peptide but not to a monolayer of SYT2 with a farnesyl group (*25*) instead of the TMD domain (fig. S1), showing that this interaction was mainly driven by SYT2 TMD domain. Altogether, these experiments demonstrate that the LBL of BoNT/B directly binds to the sugar part of GT1b as well as to the TM of SYT.

SYT1H_{51}/K_{52} and SYT2-N_{59}/K_{60} are key residues in BoNT/B binding

We have previously shown that the mutation SYT1-K_{52}A abolished BoNT/B binding to PC12 neuroendocrine cells (*25*). Our present molecular modeling data predicts that, upon toxin binding, a molecular rearrangement occurs in the vicinity of SYT1-K_{52} and the corresponding SYT2-K_{60}. We thus investigated whether the SYT2-K_{60} was also an important determinant in BoNT/B binding. Surface Plasmon Resonance analysis indicated that binding of the SYT2-G_{40}-W_{66} peptide to GT1b-containing liposomes was drastically inhibited by mutating K_{60} to alanine (figs. S1 and S9), showing that SYT2-K_{60} residue is involved in the SYT2/GT1b interaction like SYT1-K_{52} (*25*). Immunofluorescence experiments showed that BoNT/B binding was severely impaired in PC12 cells expressing SYT2-K_{60}A, compared to cells expressing SYT2-WT, with a decrease of 64 % (fig. S10A, C). A similar degree of inhibition (69%) was obtained using HEK 293 cells (fig. S10B, D). Although this decrease is less than that observed for SYT1-K_{52}A (*25*), these results indicate that the SYT2-K_{60}A like SYT1-K_{52}, is an important determinant in BoNT/B binding.

According to our model, SYT1-H_{51} and SYT2-N_{59} residues adjacent to SYT1-K_{52} and SYT2-K_{60} respectively, exhibit a high energy of interaction with BoNT/B (Fig. 3, fig. S6, Table S2). To ascertain the functional involvement of SYT1-H_{51} in BoNT/B binding to SYT1, we mutated SYT1-H_{51} to a glycine residue and measured by immunofluorescence BoNT/B binding to either WT or SYT1 mutant transfected HEK 293 cells. The mutation SYT1-H_{51}G induced a significant reduction

(35%) in the binding of BoNT/B to the cell surface (IR BoNT/B of SYT1-WT: 1.00 ± 0.04 vs. IR BoNT/B of SYT1-H_{51}G: 0.65 ± 0.04) while it did not affect expression levels of SYT1 (IR SYT of SYT1-WT: 1.00 ± 0.02 vs. IR SYT of SYT1-H_{51}G: 1.01 ± 0.02) (Fig. 7A). Interestingly, a variant of SYT2-N_{59} (SYT2-N_{59}Q) occurs naturally in cats, which are known to be resistant to type B botulism (*31*), while expressing cleavable VAMP1, the predominant VAMP isoform in motor neurons (*6*) (Table S5). Of note, a Q residue at position 59 was present in all Felidae sequences analyzed (Table S5). Felidae are primarily or opportunistically scavengers, feeding on carrion, a major vector of botulism (*32*). Given the position of N_{59} and its potential interactions with the toxin, N_{59}Q substitution may induce steric hindrance impacting the binding of BoNT/B to SYT2. In order to address the accuracy of the present model and evaluate the potential impact on BoNT/B binding of this naturally occurring mutation, we transfected HEK 293 cells with either SYT2-WT or SYT2-N_{59}Q and investigated by immunofluorescence BoNT/B binding in the presence of GT1b. As shown in Fig. 7, the N_{59}Q mutation induced a 50% decrease in BoNT/B binding (IR BoNT/B of SYT2-WT: 1.00 ± 0.03 vs. IR BoNT/B of SYT2-N_{59}Q: 0.52 ± 0.02), while the expression of SYT2 remained unaffected (IR SYT of SYT2-WT: 1.00 ± 0.01 vs. IR SYT of SYT2-N_{59}Q: 0.96 ± 0.01). Taken together, these results indicate that both SYT1-$H_{51}K_{52}$ and SYT2-$N_{59}K_{60}$ homologous residues constitute a crucial doublet for BoNT/B binding, and are consistent with the proposed structure of the SYT/GT1b/GD1a/cholesterol/BoNT-B complex. They also provide an evolutionary explanation for the appearance of mutations (SYT2-N_{59}Q) in animals with a diet at least partially based on carrion.

Discussion

The current view of the BoNT/B binding determinants that anchor the distal tip of BoNT/B C-terminal domain to nerve terminals consists of two closed pockets interacting independently with SYT and gangliosides (GT1b or GD1a), and a lipid-binding loop thought to interact with the cell membrane via hydrophobic interactions. The central role of SYT in BoNT/B toxicity is supported by its relatively high affinity for the toxin, its synaptic localization conferring tissue specificity and by the observation that changes in potency among different BoNT/B isotypes are related to variability in the BoNT/B domain recognizing SYT but not in GBS1 (*2*) (*33*). Accordingly, the human SYT2-F_{54}L variant shows a reduction in BoNT/B affinity and toxicity compared to mouse. In addition, a single or dual point mutation in the SYT binding pocket of recombinant BoNT/B increases its binding affinity to neuronal membrane and improves its clinical efficacy in a murine model (*6*).

Functional assays have unambiguously demonstrated that gangliosides are also necessary for BoNT/B intoxication and GT1b has a drastic synergistic effect on BoNT/B binding to SYT-containing membranes (*25*) (*24*) (*27*) (*21*). However, the contribution of GT1b to neuronal membrane recognition by BoNT/B, is not totally understood. The affinity of the toxin for GT1b reconstituted in nanodiscs is weak (30-50 µM) (*14*) (*15*) and not sufficient to measure detectable BoNT/B binding and VAMP2 cleavage in SYT knockout hippocampal neurons (*34*). Yet, both the canonical ganglioside binding site GBS1 and the LBL appear to participate in GT1b potentiation of BoNT/B binding to SYT, as inactivation of the GBS1 or the LBL abolish the synergistic effect of GT1b in vitro and cause a strong reduction of toxicity (*27*) (*15*).

In a recent study we elucidated an important new mechanism underlying the role of gangliosides by demonstrating that GT1b actually binds to SYT JMD and induces the formation of an alpha-helix from an initially disordered domain (*25*). Intriguingly, GT1b overlaps critical residues defined by crystallographic and biochemical experiments in the SYT2-F_{54}-I_{58} region, raising the question whether and how BoNT/B recognizes a preassembled GT1b/SYT complex and whether this complex dissociates upon BoNT/B binding (*25*).

Several experimental methods have been used to analyze the synergetic effect of GT1b on BoNT/B binding to SYT, including cultured cells and reconstituted systems (proteoliposomes, ELISA, mixed detergent micelles) (*25*) (*24*) (*27*) (*35*). However, these approaches were not adapted to assessing whether during the GT1b potentiation effect, SYT is associated with GT1b. In the present study, we developed a SPR binding assay, with several GT1b molecules engaged in a complex with SYT, ensuring that BoNT/B could recognize SYT complexed to GT1b, along with free GT1b molecules that could also interact with the ganglioside-binding pocket of the toxin. This protocol revealed that a synergistic effect occurs when GT1b is bound to SYT, which is comparable to that observed when SYT is reconstituted in liposomes containing GT1b (*25*). Altogether, the SPR data strongly suggested that the SYT binding pocket of BoNT/B can accommodate SYT bound to GT1b.

We then used molecular modeling to assess how BoNT/B could recognize the SYT/GT1b complex. We docked the SYT/GT1b complex into the BoNT/B SYT-binding pocket, based on the co-crystal coordinates of BoNT/B associated with GD1a, together with the membrane-embedded domains of SYT and gangliosides. Cholesterol, which is known to interact with both the TM of SYT and the ceramide moiety of gangliosides (*36*) was also included in the system. Docking simulations revealed that BoNT/B bound to GD1a can also interact with SYT1 or SYT2 bound to GT1b via the BoNT/B SYT-binding pocket described by structural data. The BoNT/B residues interacting either with SYT or GT1b are overall the same as described in the crystal structure, yet with additional interactions in the N-terminal domain of SYT. The SYT helix pre-conformed by GT1b extends

from E_{44} to N_{59} and the BoNT/B-SYT interaction is mainly driven by apolar residues, including SYT2-F_{47}, F_{54}, F_{55} and I_{58} as previously described (*21*) (*20*). The membrane constraints of our present model, introduce an angle between SYT and the membrane plane, modifying the interaction map between BoNT/B and the SYT helix in comparison to structural data obtained with only the extracellular domain of SYT (*21*) (*20*) (*22*). It is of note that GT1b rescue of BoNT/B binding to several SYT mutants have revealed the crucial role of SYT2-F_{54} at the BoNT/B-SYT interface (*21*) (*20*) (*37*). Interestingly, our proposed models support this observation since they show that SYT2-F_{54} and its counterpart SYT1-F_{46} strongly interact with both GT1b and BoNT/B. Thus, molecular modeling, along with SPR binding experiments, are consistent with the view that the SYT/GT1b complex does not dissociate upon BoNT/B interaction and is recognized by the SYT binding pocket.

Our modeling and experimental data reveal that SYT2 (I_{58}-W_{66}) and SYT1 (L_{50}-W_{58}) regions, just upstream of the TMD of SYT, could play a pivotal role in the BoNT/B binding mechanism. The LBL binds to this region via several apolar residues and mutation of N_{59} and K_{60} in SYT2 (H_{51} and K_{52} in SYT1) inhibited binding of BoNT/B. Furthermore, several molecular rearrangements are predicted to occur in this domain namely for SYT1-K_{52}-I_{53} and SYT2-K_{60}-I_{61} which tend to lose interaction energy with GT1b for the benefit of BoNT/B.

During the minimization process the BoNT/B LBL moves toward SYT/GT1b so that it finally interacts with sialic acids of GT1b, the extracellular C-terminal part of the SYT JMD as well as membrane-embedded SYT residues. This movement of the LBL is allowed by the initial interaction with the preformed SYT/GT1b complex which determines the orientation of BoNT/B so that the LBL is directed toward the glycone part of GT1b and the TM domain of SYT. Consistent with our model, we determined experimentally that the binding of the LBL to SYT requires the presence of its TM domain. The LBL binding to SYT TM agrees with observations that a BoNT/B mutant with LBL deletion still recognizes the extracellular SYT2 domain, but displays drastically decreased binding to SYT2 with TMD, whether in the absence or presence of ganglioside (*15*). We also find that LBL directly binds to a monolayer of GT1b, but does not recognize sphingomyelin. This suggests that the LBL preferentially recognizes the polar headgroup of GT1b. The demonstration of a direct interaction between LBL and GT1b corroborates a report that LBL deletion decreased BoNT/B binding to nanodiscs containing GT1b (*15*). From a structural point of view, our findings suggest that BoNT/B LBL reinforces the interaction of BoNT/B with the SYT/GT1b receptor, explaining why its deletion dramatically reduces BoNT/B toxicity (*15*). Interestingly, BoNT/C, BoNT/D and tetanus toxin, also possess a lipid-binding loop that has been shown to bind sialic acids and it has been reported that the BoNT/C and BoNT/D LBL are structurally close to the

corresponding SYT-binding site of BoNT/B (*13*) (*30*) (*12*) (*38*). We propose that, for BoNT/B, C, D and tetanus toxin, a functional relationship exists between the presence of an LBL and the ability of these toxins to bind free or SYT-associated sialic acids outside of GBS1. As BoNT/G has a similar SYT-binding site to BoNT/B and an LBL, it would be interesting to investigate if this toxin also interacts with a SYT/GT1b complex (*37*). For BoNT/A and BoNT/E, the absence of LBL would be compensated by an interaction with glycosides covalently linked to their receptor, SV2 in this case (*1*).

In addition to the LBL, the model predicts that BoNT/B loop 1113-1117 also interacts with sialic acids of the GT1b-SYT complex. Interestingly and independently from GBS1, tetanus toxin, BoNT/C and BoNT/D use residues with a similar 3D-position to the BoNT/B 1113-1117 loop to mediate binding to sialic acids. As co-crystallization studies failed to detect the presence of sialyllactose in the BoNT/B SYT binding pocket (*39*), our model suggests that BoNT/B can bind sialic acid only when the glycoside is presented by SYT. The fact that BoNT/B could bind another ganglioside, in addition to that occupying GBS1, is compatible with the observation that trefoil recognition of carbohydrates is often multivalent (*40*). It has been noted that BoNT/B binds SYT using a pocket that is homologous to the sia-binding site of BoNT/C, BoNT/D and tetanus toxin (*12*), consistent with the view that the so-called sialic acid site of other BoNTs and the SYT binding site of BoNT/B may have a structurally related conserved function (*12*). Our model indicates that this pocket has conserved its ability to bind sialic acid associated with SYT in the case of BoNT/B. Thus, instead of the predominant view that BoNTs independently recognize a protein and a ganglioside or two gangliosides (BoNT/C) using two distinct pockets, our data support a new scenario in which a BoNT protein-binding pocket accepts a preformed protein/ganglioside complex. To our knowledge, this is the first description of recognition by a toxin of a protein/ganglioside complex.

Our model significantly extends our understanding of the BoNT/B-SYT binding interface and uncovers additional interacting residues in SYT. Among them SYT2-N_{59} and its SYT1-H_{51} counterpart were predicted to engage strong interactions with BoNT/B in particular with E_{1191}, a key residue that modulates engineered BoNT/B activity for therapeutic purpose. This important feature was confirmed by mutagenesis and evaluation of BoNT/B binding to SYT-expressing cell cultures. It is interesting to note that the SYT2-N_{59}Q mutation is associated with a decrease of BoNT/B binding. The presence of a glutamine at this position corresponds to a natural polymorphism in Felidae. Certain animals are resistant to botulism (*41*) (*31*) and to our knowledge type B botulism has never been reported in the Felidae. Taken together, our data may suggest that

this natural variant could confer partial protection against type B botulism in animals feeding on carrion which can contain high amounts of BoNTs (*32*).

Our current findings thus highlight a new role for GT1b in BoNT/B binding by its direct interaction with SYT, explaining the poor affinity of BoNT/B for GT1b alone, but potently enhancing binding in the presence of SYT, particularly for SYT1. The very low affinity of BoNT/B for SYT1 has been suggested to be partially due to a steric clash with the toxin, involving SYT1-L_{50} (*21*) (*42*). BoNT/B has been estimated to have at least 100-fold less affinity for SYT1 than SYT2 while GT1b reduces this difference 10-fold (*20*) (*25*). Our present model predicts that SYT1-L_{50} binds GT1b and therefore a preassembled SYT/GT1b complex may facilitate BoNT/B binding to SYT1. Moreover our results are consistent with the fact that competitive neutralization of BoNT/B toxicity requires a SYT/ganglioside mixture rather SYT alone (*26*).

Our data revisit the dual receptor model (*43*) by uncovering an additional role for GT1b. We propose a new model in which, after the toxin is attracted and concentrated on the membrane by the negative charges of GT1b in lipid rafts (*44*), a preassembled and structured SYT/GT1b complex is accommodated in the SYT-binding pocket of BoNT/B, concomitantly to the binding of a ganglioside in the conserved ganglioside binding site GBS1. The LBL would then reinforce BoNT/B binding by interacting with SYT TMD and its preassembled GT1b. Accordingly, mutations in the GBS1, lipid binding loop or perturbation of GT1b/SYT interaction result in a loss of BoNT/B affinity and toxicity (*25*) (*15*) (*27*). After internalization, GT1b would participate in the toxin translocation process (*45*).

The organization of SYT/GT1b and GD1a receptors in the model with connected intramembrane domains, mimics chalice-shaped dimers reported for alpha synuclein and beta amyloid peptide, which are also chaperoned by the head groups of gangliosides in cholesterol enriched membrane domains (*46*) (*47*) (*48*). As synaptic vesicles are highly enriched in cholesterol, it is probable that pre-assembled SYT/cholesterol complexes are translocated to the plasma membrane and are then integrated in a raft region where it can interact with GT1b and other polysialogangliosides. It has been suggested that simultaneous binding to SYT and gangliosides could impose a limited degree of freedom on BoNT/B orientation with respect to the membrane surface (*20*) (*49*). In line with this notion, our data suggest that the intramembrane interactions between SYT and gangliosides could indeed immobilize both co-receptors at an appropriate distance, optimizing binding.

In summary, we present here a model of BoNT/B binding to neuronal membranes, that takes into account the specific topology of membrane receptors. BoNT/B has been successfully engineered to increase its affinity in a preclinical model (*6*). Our present findings could provide insights into the

rational design of recombinant BoNTs for medical applications and for the development of inhibitors (*50*) (*51*) (*14*).

Materials and Methods

Experimental design

The main objective of this study was to investigate how botulinum neurotoxin serotype B binds to its receptors in a membrane context, since the available structural data were obtained in the absence of apolar domains. We developed an SPR (Surface Plasmon Resonance) experimental configuration to ensure that the synaptotagmin domain that interacts with BoNT/B was bound to GT1b, before characterizing the interaction of BoNT/B with this preassembled complex. Molecular modeling was performed to model BoNT/B in interaction with the preassembled SYT1/GT1b and SYT2/GT1b complexes docked to the synaptotagmin binding pocket. For this purpose, we used the structural coordinates stored in the PDB files 6G5K, 4KBB and 2NP0 to generate a complete model of BoNT/B-SYT1/2-gangliosides and cholesterol. We compared the interaction energies and landscapes of all components of the complexes with previous structural data. Newly identified contact points were compared with published reports and the importance of new synaptotagmin-contact points were experimentally validated in heterologous expression systems.

Reagents

BoNT/B (B1 Okra strain) was obtained as described (*25*). All peptides were synthesized by Genecust, except for farnesylated pSYT2 (*25*). DMPC (1,2-Dimyristoyl-sn-glycero-3-phosphocholine) was from Avanti Polar Lipids. GT1b was from Matreya LLC. Polyclonal anti-SYT1 31-55 region antibodies were generously provided by M. Takahashi. Rabbit anti-SYT2 40-65 polyclonal antibodies were produced by Genecust using a synthetic peptide (rat SYT2 40-65) and purified using protein-A sepharose. All experiments were performed in accordance with French and European guidelines for handling botulinum neurotoxin. GT1b, lyso-lactosylceramide and sphingomyelin were from Matreya LLC. Anti-BoNT/B and anti-SYT1/2 (1D12) antibodies were obtained as described (*25*). Alexa-coupled secondary antibodies were from Jackson Immunoresearch. DAPI was from SIGMA-Aldrich. Anti-GT1b monoclonal antibodies were from Merck Millipore (MAB 5608).

SPR experiments

SPR measurements were performed with a Biacore T200 apparatus (Cytiva) using HBS (10 mM HEPES/NaOH pH 7.4, 150 mM NaCl) or TBS (10 mM TRIS/NaOH pH 7.4, 150 mM NaCl) as running buffer. CMDP chips (Xantec Bioanalytics, Germany) were functionalized with neutravidin (Pierce) according to standard protocols. pSYT peptides were injected onto neutravidin to reach between 250-500 RU, depending on the experiment. GT1b (2 mg/ml in methanol) was diluted extemporaneously in running buffer and injected onto pSYT sensorchips at flow rates from 5 to 40 µl/min, depending on experiments. Gangliosides were stripped from pSYT using TBS containing CHAPS 1% (8 s at 40 µl/min). The binding stoichiometry of GT1b/pSYT was calculated using the RUmax value, determined experimentally by saturating pSYT with GT1b diluted under the CMC (10 µM) (*28*). Stoichiometry = RU_{max} x MW of GT1b / RU pSYT x MW of pSYT). BoNT/B was injected at 30 nM at a flow rate of 5 µl/min. For GT1b potentiation of BoNT/B binding to pSYT1, GT1b was not stripped and accumulated on pSYT1 after each BoNT/B injection. Anti-GT1b antibodies (ascite, dilution x 1000) were injected for 2 min at 10 µl/min over pSYT1 and pSYT1/GT1b complex (250 RU pSYT1 ± GT1b (30-100 RU)), before and after BoNT/B interaction (20 nM for 3 min). Unless stated, non-specific signals on control flow cells (immobilized pSYT9 or activated / deactivated empty flow cell) were automatically subtracted from measurements on experimental flow cells. Measurement of pSYT2 peptide binding to GT1b-containing liposomes was performed using hydrophobic L1 sensor chips as described (*25*). Liposomes containing 100 % DMPC (control flow cell) or 92 % DMPC, 8% GT1b (experimental flow cell) were immobilized and SYT2 peptides binding measured 5 s before the end of the injection.

Langmuir monolayers experiments

Surface pressure measurements revealing peptide-lipid and peptide-peptide interactions at the air-water interface were studied by the Langmuir film balance technique with a fully automated microtensiometer (µTROUGH SX, Kibron Inc. Helsinki, Finland) as described previously (*52*) (*53*) (*25*).

Immunofluorescence

HEK293 or PC12 cells, were cultured on poly-L-Lysine (10 µg/ml) treated coverslips (300,000 cells per well) in DMEM containing 5% FBS, 5% HS and 1% penicillin/streptomycin mixture (complete medium). Cells were transfected with the corresponding plasmids (pIRES-EGFP-SYT2; pIRES-EGFP-K_{60}A-SYT2; pIRES-EGFP-N_{59}Q-SYT2; pIRES-EGFP-SYT1 or pIRES-EGFP-H_{51}G-SYT1) using Lipofectamine 2000 and according to the manufacturer's procedure. 40 hours

after transfection, GT1b (10 µg/ml) was added to the wells in DMEM and incubated for 1.5 h at 37°C followed by one washing step and transfer to complete medium. BoNT/B (10 nM and 1 nM for SYT1 and SYT2 conditions respectively) was added afterwards and incubated for 30-45 min at 37°C. After a first wash with the culture medium, additional washes were performed with PBS and cells were fixed in the dark at 4°C in 4% paraformaldehyde/PBS for 15 min followed by NH_4Cl washing steps. Non-specific binding was blocked with 0.2% (w/v) gelatine or 5% (v/v) goat serum in a PBS buffer containing 0.1% saponin. Anti-BoNT/B (0.5 µg/µl), and 1D12 anti-SYT (1 µg/ml) antibodies were then added for 45 min at 22°C. After subsequent washing, staining was visualized using secondary anti-rabbit Alexa-594 and anti-mouse Alexa-488 antibodies. Nuclei were detected using DAPI.

Image acquisition and analysis

Confocal images were acquired on a Zeiss LSM780 microscope and processed using ImageJ (http://rsb.info.nih.gov/ij/). For quantification, SYT immunolabeling images were thresholded in order to get a binary mask. This binary mask was used to obtain immunoreactivity (IR) values of the regions of interest (ROIs) over SYT and BoNT/B channels. For comparisons of BoNT/B binding to WT vs mutant SYTs, IR values were normalized to WT in every experiment. Results are presented as mean ± SEM. Statistical analysis was performed using Mann-Whitney U test.

Molecular modelling

Molecular modelling studies were performed using Hyperchem (http://www.hyper.com), Deep View/Swiss-Pdb viewer (https://spdbv.vital-it.ch) and Molegro Molecular viewer (http://molexus.io/molegro-molecular-viewer) as described in previous studies (*25*) *(54)*. The coordinates of the BoNT/B Lipid binding loop (aa 1245-1252) present in PDB 2NM1 were inserted in PDBs files 4KBB and 6G5K. The sugar coordinates of GD1a were then merged with the PDB file 6G5K to reconstitute a trimolecular complex for SYT1. The preassembled complex GT1b/SYT1 and GT1b/SYT2 were docked on the synaptotagmin binding pocket according to the crystal coordinates of SYT1 (PDB 6G5K) and SYT2 (PDB 4KBB). The structures of the ceramide part of GD1a and cholesterol were retrieved from the platform Charmm-GUI and added to the models to obtain a full system in a membrane context. Energy minimization was performed with the Polak-Ribière conjugate gradient algorithm, with the Bio+(CHARMM) force field in Hyperchem, typically with 3×10^5 steps, and a root-mean-square (RMS) gradient of 0.01 kcal. $Å^{-1}.mol^{-1}$ as the convergence condition.

In order to generate a schematic representation of the membrane-embedded protein complexes, we used CHARM-GUI membrane builder (*55*) by inserting protein complexes previously oriented in the PPM Web Server (*56*). The protein complex was embedded in a 128-DPPC (1,2-Dipalmitoylphosphatidylcholine) molecule bilayer. For visual clarity, and since the membrane-embedded protein complexes were not used for any further calculations, some of the DPPC molecules around the protein complexes were manually erased in order to have a better perspective of the regions of interest in the BoNT/B-synaptotagmin complexes. In fig. S4A, only the phosphate groups of the DPPCs were depicted so as to have a visual reference of the membrane plane. Figures of the protein complexes inserted in the membrane systems were generated using Chimera software *(57)*.

Statistical analysis

Results are presented as mean ± SEM of n independent experiments. Statistical analysis was performed using either Mann-Whitney U test or One-way ANOVA followed by Bonferroni post-hoc test for means comparisons. All statistical tests were performed using OriginPro 8.0.

References

1. B. Poulain, E. Lemichez, M. R. Popoff, Neuronal selectivity of botulinum neurotoxins. *Toxicon* **178**, 20-32 (2020).
2. M. Dong, G. Masuyer, P. Stenmark, Botulinum and Tetanus Neurotoxins. *Annu Rev Biochem* **88**, 811-837 (2019).
3. J. R. Davies, S. M. Liu, K. R. Acharya, Variations in the Botulinum Neurotoxin Binding Domain and the Potential for Novel Therapeutics. *Toxins (Basel)* **10**, (2018).
4. S. Pellett, T. L. Yaksh, R. Ramachandran, Current status and future directions of botulinum neurotoxins for targeting pain processing. *Toxins (Basel)* **7**, 4519-4563 (2015).
5. M. Pirazzini, O. Rossetto, R. Eleopra, C. Montecucco, Botulinum Neurotoxins: Biology, Pharmacology, and Toxicology. *Pharmacol Rev* **69**, 200-235 (2017).
6. M. Elliott, C. Favre-Guilmard, S. M. Liu, J. Maignel, G. Masuyer, M. Beard, C. Boone, D. Carre, M. Kalinichev, S. Lezmi, I. Mir, C. Nicoleau, S. Palan, C. Perier, E. Raban, S. Zhang, M. Dong, P. Stenmark, J. Krupp, Engineered botulinum neurotoxin B with improved binding to human receptors has enhanced efficacy in preclinical models. *Sci Adv* **5**, eaau7196 (2019).
7. R. L. Schnaar, Gangliosides of the Vertebrate Nervous System. *Journal of Molecular Biology* **428**, 3325-3336 (2016).
8. S. Sipione, J. Monyror, D. Galleguillos, N. Steinberg, V. Kadam, Gangliosides in the Brain: Physiology, Pathophysiology and Therapeutic Applications. *Front Neurosci* **14**, 572965 (2020).
9. M. Zuverink, J. T. Barbieri, Protein Toxins That Utilize Gangliosides as Host Receptors. *Prog Mol Biol Transl Sci* **156**, 325-354 (2018).
10. J. Fantini, N. Yahi, Eds., *Brain Lipids in Synaptic Function and Neurological Disease : Clues to Innovative Therapeutic Strategies for Brain Disorders*, (Elsevier Academic Press, New-York 2015), vol. 2015, pp. 398.

11. J. Fantini, H. Chahinian, N. Yahi, Synergistic antiviral effect of hydroxychloroquine and azithromycin in combination against SARS-CoV-2: What molecular dynamics studies of virus-host interactions reveal. *Int J Antimicrob Agents* **56**, 106020 (2020).
12. A. P. Karalewitz, Z. Fu, M. R. Baldwin, J. J. Kim, J. T. Barbieri, Botulinum neurotoxin serotype C associates with dual ganglioside receptors to facilitate cell entry. *J Biol Chem* **287**, 40806-40816 (2012).
13. J. Strotmeier, K. Lee, A. K. Volker, S. Mahrhold, Y. Zong, J. Zeiser, J. Zhou, A. Pich, H. Bigalke, T. Binz, A. Rummel, R. Jin, Botulinum neurotoxin serotype D attacks neurons via two carbohydrate-binding sites in a ganglioside-dependent manner. *Biochem J* **431**, 207-216 (2010).
14. L. Yin, G. Masuyer, S. Zhang, J. Zhang, S. I. Miyashita, D. Burgin, L. Lovelock, S. F. Coker, T. M. Fu, P. Stenmark, M. Dong, Characterization of a membrane binding loop leads to engineering botulinum neurotoxin B with improved therapeutic efficacy. *PLoS Biol* **18**, e3000618 (2020).
15. D. Stern, J. Weisemann, A. Le Blanc, L. von Berg, S. Mahrhold, J. Piesker, M. Laue, P. B. Luppa, M. B. Dorner, B. G. Dorner, A. Rummel, A lipid-binding loop of botulinum neurotoxin serotypes B, DC and G is an essential feature to confer their exquisite potency. *PLoS Pathog* **14**, e1007048 (2018).
16. C. Chen, M. R. Baldwin, J. T. Barbieri, Molecular basis for tetanus toxin coreceptor interactions. *Biochemistry* **47**, 7179-7186 (2008).
17. C. Thiele, M. J. Hannah, F. Fahrenholz, W. B. Huttner, Cholesterol binds to synaptophysin and is required for biogenesis of synaptic vesicles. *Nat Cell Biol* **2**, 42-49 (2000).
18. Y. Park, J. B. Seo, A. Fraind, A. Perez-Lara, H. Yavuz, K. Han, S. R. Jung, I. Kattan, P. J. Walla, M. Choi, D. S. Cafiso, D. S. Koh, R. Jahn, Synaptotagmin-1 binds to PIP(2)-containing membrane but not to SNAREs at physiological ionic strength. *Nat Struct Mol Biol* **22**, 815-823 (2015).
19. J. Yao, S. E. Kwon, J. D. Gaffaney, F. M. Dunning, E. R. Chapman, Uncoupling the roles of synaptotagmin I during endo- and exocytosis of synaptic vesicles. *Nat Neurosci* **15**, 243-249 (2011).
20. R. Jin, A. Rummel, T. Binz, A. T. Brunger, Botulinum neurotoxin B recognizes its protein receptor with high affinity and specificity. *Nature* **444**, 1092-1095 (2006).
21. Q. Chai, J. W. Arndt, M. Dong, W. H. Tepp, E. A. Johnson, E. R. Chapman, R. C. Stevens, Structural basis of cell surface receptor recognition by botulinum neurotoxin B. *Nature* **444**, 1096-1100 (2006).
22. R. P. Berntsson, L. Peng, M. Dong, P. Stenmark, Structure of dual receptor binding to botulinum neurotoxin B. *Nat Commun* **4**, 2058 (2013).
23. R. Desplantes, C. Leveque, B. Muller, M. Lotierzo, G. Ferracci, M. Popoff, M. Seagar, R. Mamoun, O. El Far, Affinity biosensors using recombinant native membrane proteins displayed on exosomes: application to botulinum neurotoxin B receptor. *Sci Rep* **7**, 1032 (2017).
24. S. Kozaki, Y. Kamata, S. Watarai, T. Nishiki, S. Mochida, Ganglioside GT1b as a complementary receptor component for Clostridium botulinum neurotoxins. *Microb Pathog* **25**, 91-99 (1998).
25. A. Flores, J. Ramirez-Franco, R. Desplantes, K. Debreux, G. Ferracci, F. Wernert, M. P. Blanchard, Y. Maulet, F. Youssouf, M. Sangiardi, C. Iborra, M. R. Popoff, M. Seagar, J. Fantini, C. Leveque, O. El Far, Gangliosides interact with synaptotagmin to form the high-affinity receptor complex for botulinum neurotoxin B. *Proc Natl Acad Sci U S A* **116**, 18098-18108 (2019).

26. M. Dong, D. A. Richards, M. C. Goodnough, W. H. Tepp, E. A. Johnson, E. R. Chapman, Synaptotagmins I and II mediate entry of botulinum neurotoxin B into cells. *J Cell Biol* **162**, 1293-1303 (2003).
27. A. Rummel, T. Eichner, T. Weil, T. Karnath, A. Gutcaits, S. Mahrhold, K. Sandhoff, R. L. Proia, K. R. Acharya, H. Bigalke, T. Binz, Identification of the protein receptor binding site of botulinum neurotoxins B and G proves the double-receptor concept. *Proc Natl Acad Sci U S A* **104**, 359-364 (2007).
28. B. Ulrich-Bott, H. Wiegandt, Micellar properties of glycosphingolipids in aqueous media. *J Lipid Res* **25**, 1233-1245 (1984).
29. J. Fantini, N. Garmy, R. Mahfoud, N. Yahi, Lipid rafts: structure, function and role in HIV, Alzheimer's and prion diseases. *Expert Rev Mol Med* **4**, 1-22 (2002).
30. J. Strotmeier, S. Gu, S. Jutzi, S. Mahrhold, J. Zhou, A. Pich, T. Eichner, H. Bigalke, A. Rummel, R. Jin, T. Binz, The biological activity of botulinum neurotoxin type C is dependent upon novel types of ganglioside binding sites. *Mol Microbiol* **81**, 143-156 (2011).
31. C. Montecucco, M. B. Rasotto, On botulinum neurotoxin variability. *MBio* **6**, (2015).
32. N. E. Ortiz, G. R. Smith, The production of Clostridium botulinum type A, B and D toxin in rotting carcasses. *Epidemiol Infect* **113**, 335-343 (1994).
33. J. R. Davies, G. Masuyer, P. Stenmark, Structural and Biochemical Characterization of Botulinum Neurotoxin Subtype B2 Binding to Its Receptors. *Toxins (Basel)* **12**, (2020).
34. M. Dong, W. H. Tepp, H. Liu, E. A. Johnson, E. R. Chapman, Mechanism of botulinum neurotoxin B and G entry into hippocampal neurons. *J Cell Biol* **179**, 1511-1522 (2007).
35. E. Wild, U. Bonifas, J. Klimek, J. H. Trosemeier, B. Kramer, B. Kegel, H. A. Behrensdorf-Nicol, In vitro potency determination of botulinum neurotoxin B based on its receptor-binding and proteolytic characteristics. *Toxicol In Vitro* **34**, 97-104 (2016).
36. J. Fantini, C. Di Scala, C. J. Baier, F. J. Barrantes, Molecular mechanisms of protein-cholesterol interactions in plasma membranes: Functional distinction between topological (tilted) and consensus (CARC/CRAC) domains. *Chem Phys Lipids* **199**, 52-60 (2016).
37. P. Stenmark, M. Dong, J. Dupuy, E. R. Chapman, R. C. Stevens, Crystal structure of the botulinum neurotoxin type G binding domain: insight into cell surface binding. *Journal of Molecular Biology* **397**, 1287-1297 (2010).
38. P. Emsley, C. Fotinou, I. Black, N. F. Fairweather, I. G. Charles, C. Watts, E. Hewitt, N. W. Isaacs, The structures of the H(C) fragment of tetanus toxin with carbohydrate subunit complexes provide insight into ganglioside binding. *J Biol Chem* **275**, 8889-8894 (2000).
39. S. Swaminathan, S. Eswaramoorthy, Structural analysis of the catalytic and binding sites of Clostridium botulinum neurotoxin B. *nature structural biology* **7**, 693-699 (2000).
40. A. P. Karalewitz, A. R. Kroken, Z. Fu, M. R. Baldwin, J. J. Kim, J. T. Barbieri, Identification of a unique ganglioside binding loop within botulinum neurotoxins C and D-SA. *Biochemistry* **49**, 8117-8126 (2010).
41. E. van Ermengem, Classics in infectious diseases. A new anaerobic bacillus and its relation to botulism. E. van Ermengem. Originally published as "Ueber einen neuen anaeroben Bacillus und seine Beziehungen zum Botulismus" in Zeitschrift fur Hygiene und Infektionskrankheiten 26: 1-56, 1897. *Rev Infect Dis* **1**, 701-719 (1979).
42. K. H. Lam, G. Yao, R. Jin, Diverse binding modes, same goal: The receptor recognition mechanism of botulinum neurotoxin. *Prog Biophys Mol Biol* **117**, 225-231 (2015).
43. C. Montecucco, How do tetanus and botulinum toxins bind to neuronal membranes? *Trends Biochem Sci* **11**, 314-317 (1986).
44. F. Fogolari, S. C. Tosatto, L. Muraro, C. Montecucco, Electric dipole reorientation in the interaction of botulinum neurotoxins with neuronal membranes. *FEBS Lett* **583**, 2321-2325 (2009).

45. S. Sun, S. Suresh, H. Liu, W. H. Tepp, E. A. Johnson, J. M. Edwardson, E. R. Chapman, Receptor binding enables botulinum neurotoxin B to sense low pH for translocation channel assembly. *Cell Host Microbe* **10**, 237-247 (2011).
46. J. Fantini, N. Yahi, N. Garmy, Cholesterol accelerates the binding of Alzheimer's beta-amyloid peptide to ganglioside GM1 through a universal hydrogen-bond-dependent sterol tuning of glycolipid conformation. *Front Physiol* **4**, 120 (2013).
47. J. Fantini, H. Chahinian, N. Yahi, Progress toward Alzheimer's disease treatment: Leveraging the Achilles' heel of Abeta oligomers? *Protein Sci* **29**, 1748-1759 (2020).
48. N. Yahi, C. Di Scala, H. Chahinian, J. Fantini, Innovative treatment targeting gangliosides aimed at blocking the formation of neurotoxic alpha-synuclein oligomers in Parkinson's disease. *Glycoconj J*, (2021).
49. R. M. Benoit, D. Frey, M. Hilbert, J. T. Kevenaar, M. M. Wieser, C. U. Stirnimann, D. McMillan, T. Ceska, F. Lebon, R. Jaussi, M. O. Steinmetz, G. F. Schertler, C. C. Hoogenraad, G. Capitani, R. A. Kammerer, Structural basis for recognition of synaptic vesicle protein 2C by botulinum neurotoxin A. *Nature* **505**, 108-111 (2014).
50. C. Rasetti-Escargueil, M. R. Popoff, Engineering Botulinum Neurotoxins for Enhanced Therapeutic Applications and Vaccine Development. *Toxins (Basel)* **13**, (2020).
51. E. Fonfria, M. Elliott, M. Beard, J. A. Chaddock, J. Krupp, Engineering Botulinum Toxins to Improve and Expand Targeting and SNARE Cleavage Activity. *Toxins (Basel)* **10**, (2018).
52. J. Fantini, N. Garmy, N. Yahi, Prediction of glycolipid-binding domains from the amino acid sequence of lipid raft-associated proteins: application to HpaA, a protein involved in the adhesion of Helicobacter pylori to gastrointestinal cells. *Biochemistry* **45**, 10957-10962 (2006).
53. C. Di Scala, J. D. Troadec, C. Lelievre, N. Garmy, J. Fantini, H. Chahinian, Mechanism of cholesterol-assisted oligomeric channel formation by a short Alzheimer beta-amyloid peptide. *J Neurochem* **128**, 186-195 (2014).
54. J. Fantini, N. Yahi, F. Azzaz, H. Chahinian, Structural dynamics of SARS-CoV-2 variants: A health monitoring strategy for anticipating Covid-19 outbreaks. *J Infect* **83**, 197-206 (2021).
55. E. L. Wu, X. Cheng, S. Jo, H. Rui, K. C. Song, E. M. Davila-Contreras, Y. Qi, J. Lee, V. Monje-Galvan, R. M. Venable, J. B. Klauda, W. Im, CHARMM-GUI Membrane Builder toward realistic biological membrane simulations. *J Comput Chem* **35**, 1997-2004 (2014).
56. M. A. Lomize, I. D. Pogozheva, H. Joo, H. I. Mosberg, A. L. Lomize, OPM database and PPM web server: resources for positioning of proteins in membranes. *Nucleic Acids Res* **40**, D370-376 (2012).
57. E. F. Pettersen, T. D. Goddard, C. C. Huang, G. S. Couch, D. M. Greenblatt, E. C. Meng, T. E. Ferrin, UCSF Chimera--a visualization system for exploratory research and analysis. *J Comput Chem* **25**, 1605-1612 (2004).

Acknowledgments

We thank Raymond Miquelis for constructive discussions.

Funding:

Institut National de la Santé et de la Recherche Médicale (INSERM)

Aix-Marseille Université (AMU)

Agence Nationale de la Recherche (ANR) (grant ANR-17-CE16-0022) for the postdoctoral financial support of JRF

Ministère des Armées (AID) and Aix-Marseille Université AMU for the PhD thesis of FO

Author contributions: CL, OEF and MSeagar conceived the study. CL and OEF supervised the entire project, the experimental design, data interpretation and manuscript preparation. CL and OEF analysed and interpreted the data. JRF and CL performed immunofluorescence experiments, JRF acquired the corresponding images and performed treatment and analysis. FA performed molecular modelling and prepared with JRF molecular modelling figures. CL and GF performed SPR experiments. JF performed Langmuir monolayer experiments. YF and MSangiardi performed expression plasmids preparation and preliminary expression tests. CL performed SPR experiments. CL wrote the original draft of the manuscript. CL, FA, JF, OEF and JRF prepared the figures. MRP was involved in discussion and data analysis. All authors edited and reviewed the manuscript.

Competing interests: The authors declare that they have no competing interests.

Data and materials availability: All data needed to evaluate the conclusions in the paper are present in the paper and/or the Supplementary Materials.

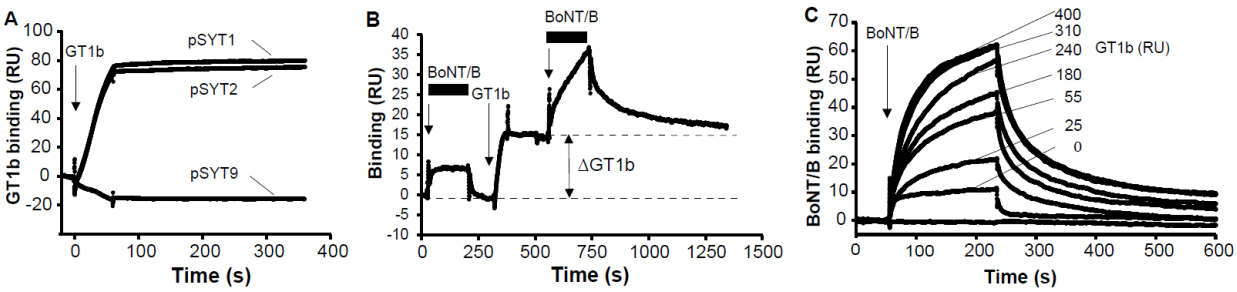

Fig.1. SPR based on-chip reconstitution of BoNT/B binding to SYT JMD pre-assembled with GT1b (**A**) GT1b binding to pSYT1 and pSYT2. GT1b (200 nM) was injected for 1 min over immobilized pSYT1, pSYT2 and pSYT9 (240 RU) at 40 µl/min. Representative of >10 independent experiments. (**B**) GT1b bound to SYT induces an increment in BoNT/B binding signal. BoNT/B (30 nM) was injected (first arrow) onto pSYT1 (260 RU) showing a transient interaction that rapidly returns to baseline level (lower dashed line). GT1b (10 nM, second arrow) was then stably immobilized on pSYT1 (ΔGT1b) generating a new baseline (upper dashed line) and BoNT/B (30 nM, third arrow) was then injected again. Black bars highlight the BoNT/B injection phases. Representative of 6 independent experiments. (**C**) GT1b potentiation of BoNT/B binding to pSYT1 depends on the amount of GT1b bound to pSYT1. Sensorgrams resulting from the interaction of BoNT/B (30 nM) with pSYT1 (300 RU) pre-assembled with various amounts of GT1b (from 0 to 400 RU) were superposed. Representative of 3 independent experiments

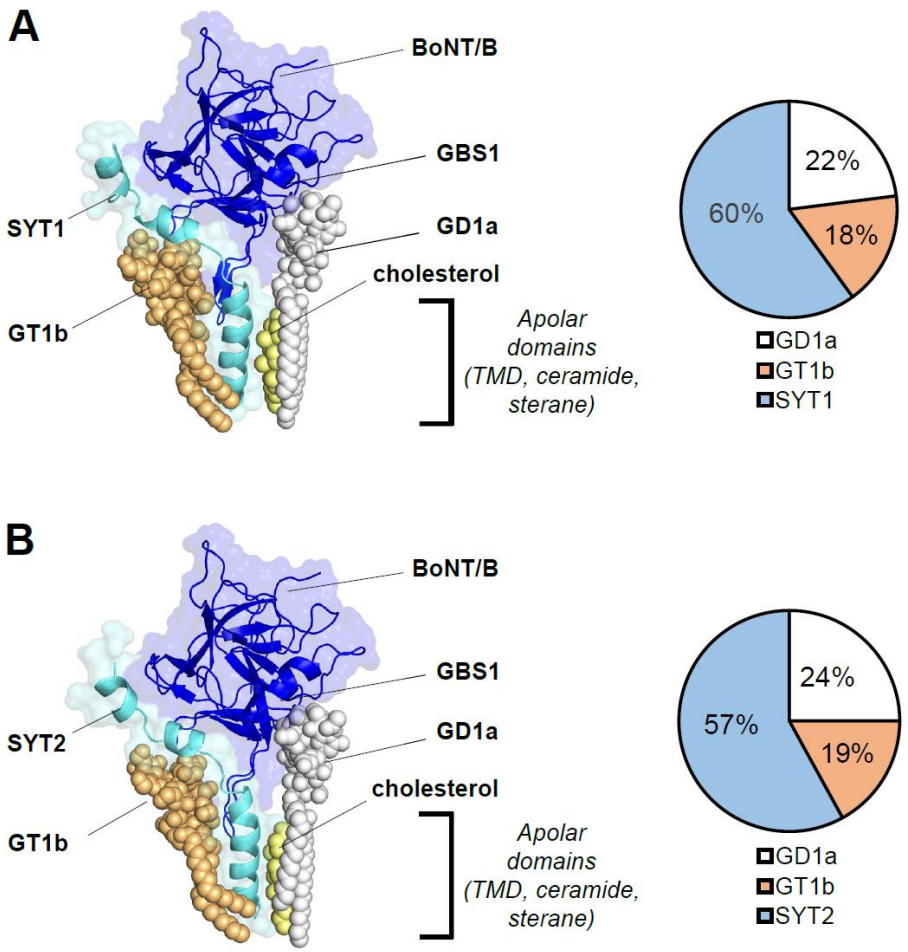

Fig. 2. Overall structure of the energy-minimized complex between BoNT/B and its membrane ligands. The models are based on the initial superposition of a preformed synaptotagmin1/2-GT1b complex positioned in the SYT binding site of the toxin, also bound to GD1a, with a cholesterol molecule positioned between SYT-TM and GD1a ceramide. (**A**) Model of SYT1-BoNT/B complex (SYT1 aa 34-72, BoNT/B HC aa 1179-1290). (**B**) Model of SYT2-BoNT/B complex (SYT2 aa 42-80, BoNT/B HC aa 1179-1290). Both BoNT/B and SYT are represented as cartoons (dark and light blue respectively). The gangliosides and cholesterol are represented as spheres (GT1b : light orange, GD1a : white , cholesterol : light yellow). The apolar domains indicated in the models correspond to the sterane and isooctyl chains of cholesterol, the ceramide part of GD1a and GT1b, and the TMD of SYT. The pie charts indicate the relative distribution of the energies of interaction in the complex between BoNT/B and SYT1, GT1b, GD1a and between BoNT/B and SYT2, GT1b, GD1a. Note that cholesterol does not interact with the toxin, but with SYT TM and the ceramide part of GD1a.

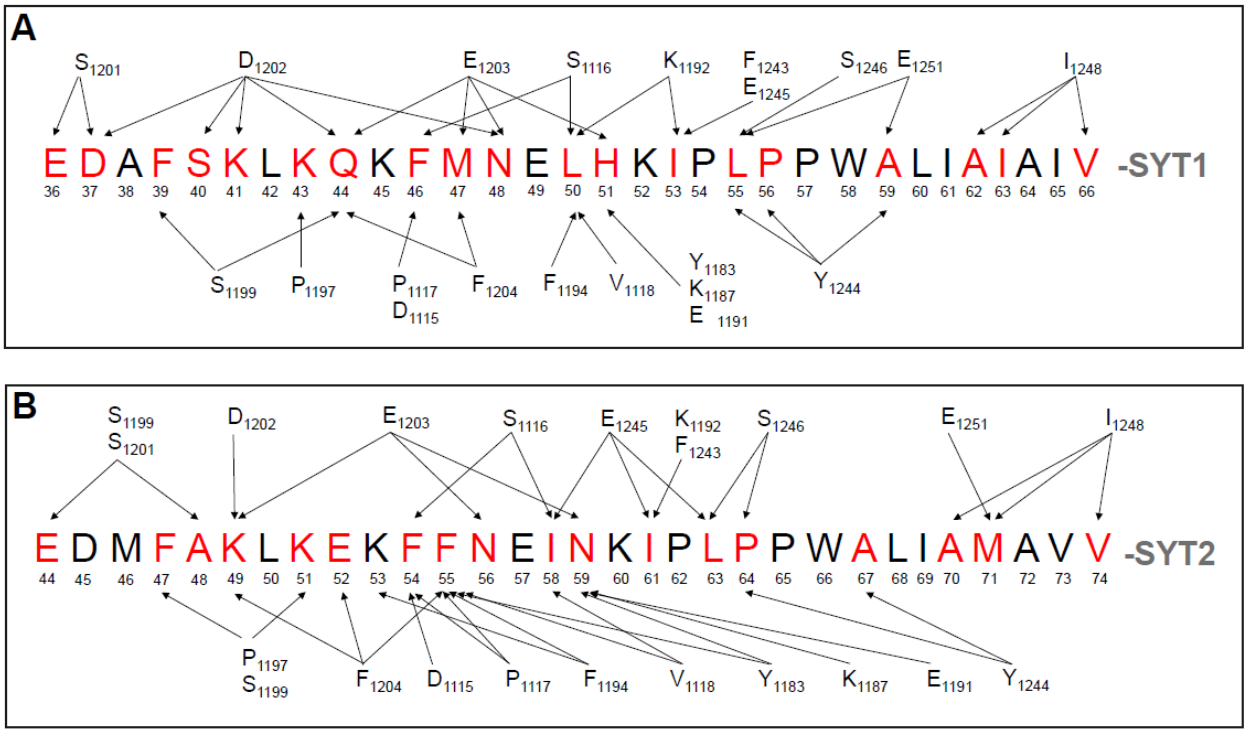

Fig. 3. Mapping of the intermolecular interactions between BoNT/B and SYT. (**A**) SYT1. (**B**) SYT2. SYT residues interacting with the toxin are highlighted in red. Arrows indicate BoNT/B-SYT interaction points. A cut off <3.5 Å was used to select the illustrated residues.

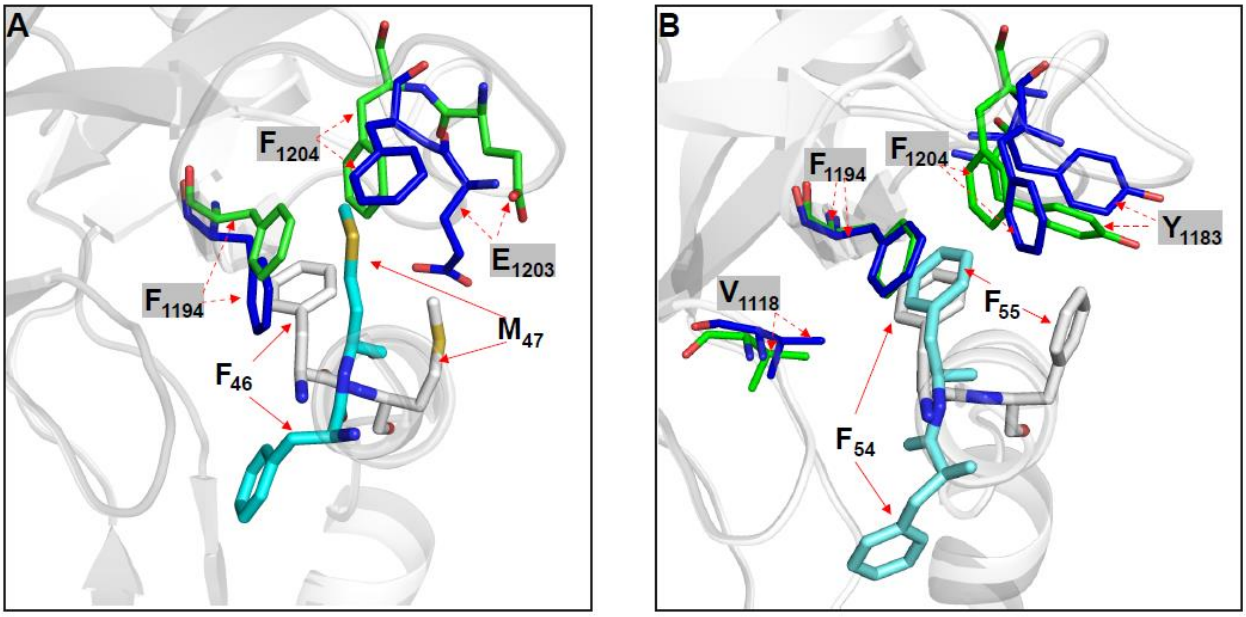

Fig. 4. Close-up view of the molecular interface of SYT1-F_{46}-M_{47} and SYT2-F_{54}-F_{55}. (**A**) Superposition of the SYT1-BoNT/B complex from PDB: 6G5K (BoNT/B in green and SYT1 in white) and the present model (BoNT/B in blue and SYT1 in light blue). (**B**) Superposition of the SYT2-BoNT/B complex from PDB 2NP0 (BoNT/B in green and SYT2 in white) and the present model (BoNT/B in blue and SYT2 in light blue). Interacting BoNT/B residues are shadowed in grey. Note that the position of BoNT/B residues are conserved between the proposed models and the corresponding crystal structures while their relative partners shift from F_{46} to M_{47} in SYT1 and F_{54} to F_{55} in SYT2.

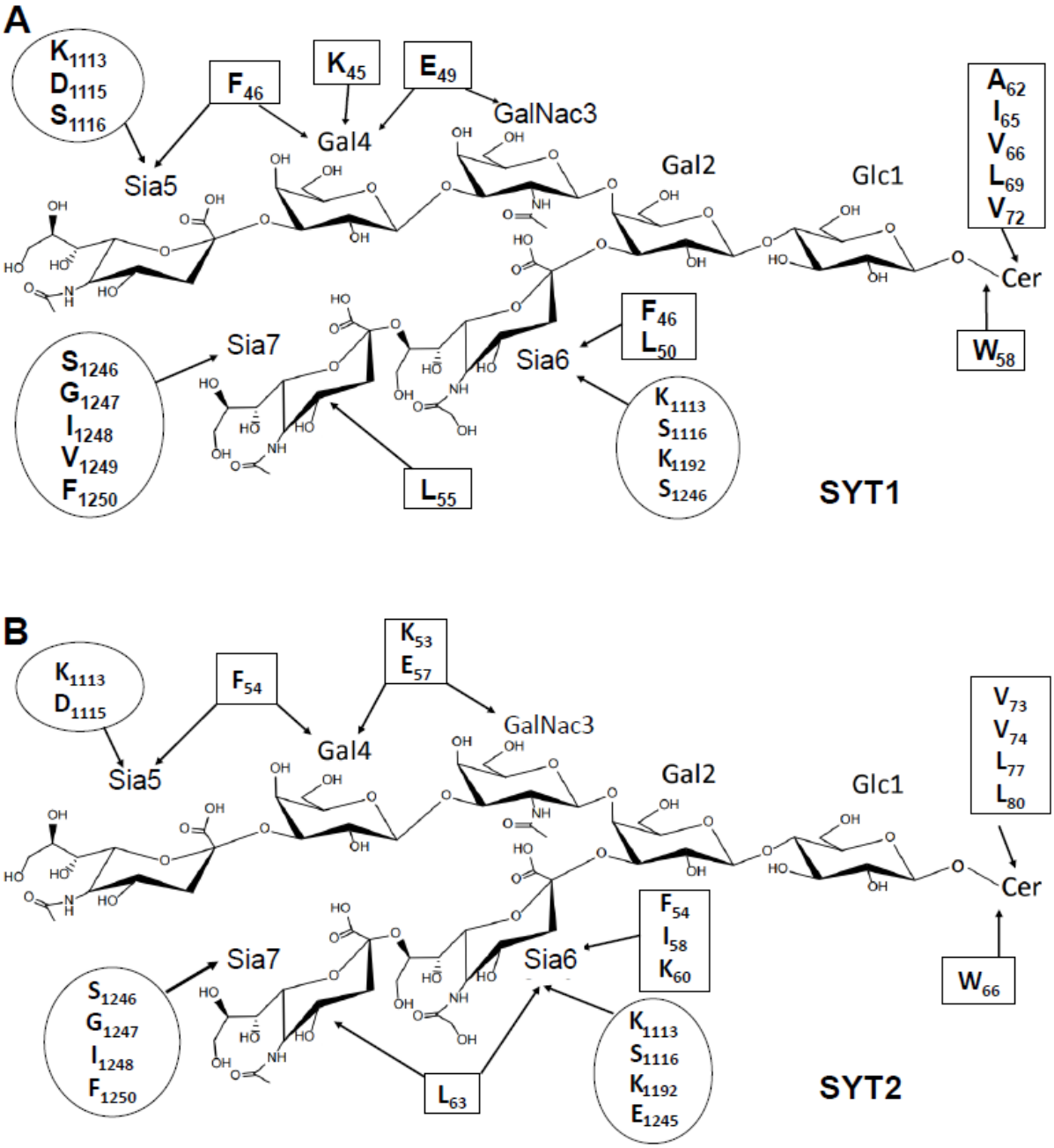

Fig. 5. Schematic overview of intermolecular interactions between GT1b-BoNT/B and GT1b-SYT. (**A**) SYT1. (**B**) SYT2. The amino acids of SYT are boxed while those of the toxin are circled. A cut off <3.5 Å was used to select the residues indicated in the figure. Glc = glucose, Gal= galactose, Gal-Nac= N- acetylgalactosamine, Sia= sialic acid, Cer = ceramide. Only residues with energy ≥ 3 kJ/mol are listed

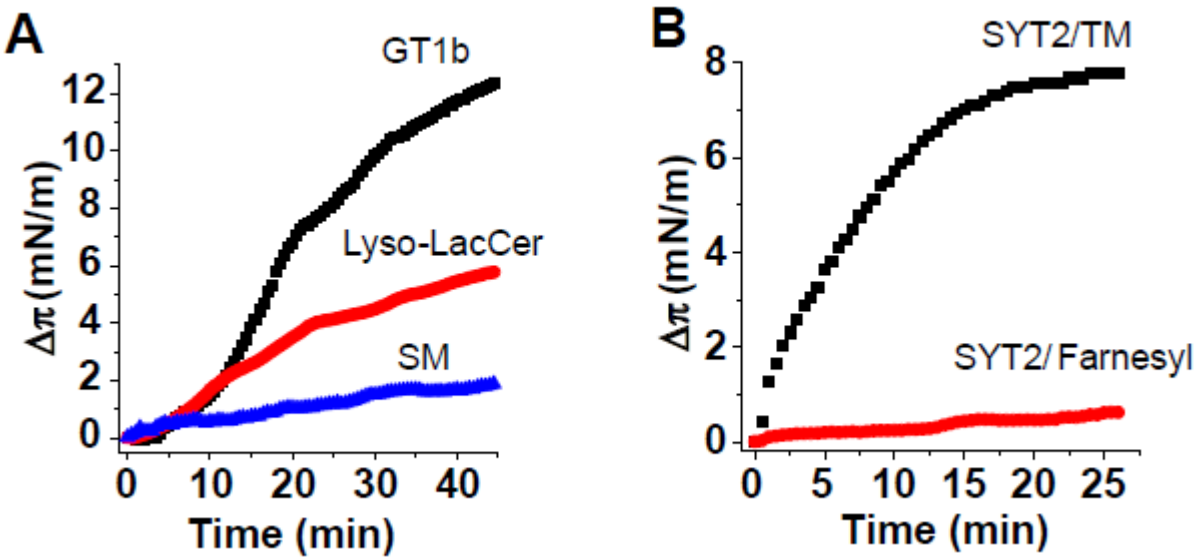

Fig. 6. **Measurement of BoNT/B apolar loop (LBL) interaction with GT1b and SYT using Langmuir monolayers.** (**A**) Stable monolayers of GT1b, lyso-LacCer, and sphingomyelin (SM) were prepared at the air-water interface at an initial surface pressure of 15-20 $mN.m^{-1}$. After equilibrium of the monolayer, the BoNT/B apolar loop (aa 1242-1256) was added at a final concentration of 10 μM. The data show the surface pressure increase Δπ induced by the loop as a function of time. The data are representative of three distinct experiments. (**B**) A biotinylated SYT2 peptide encompassing the juxtamembrane domain of SYT as well as the SYT2 transmembrane domain (aa 40-87) was prepared as a stable monolayer at the air-water interface and then incubated with the synthetic toxin apolar loop peptide (p1242-1256; 10 μM). A SYT2 peptide with a farnesyl group instead of the TM was used as control. The data show the surface pressure increases Δπ induced by the BoNT/B apolar loop as a function of time. The data are representative of three distinct experiments.

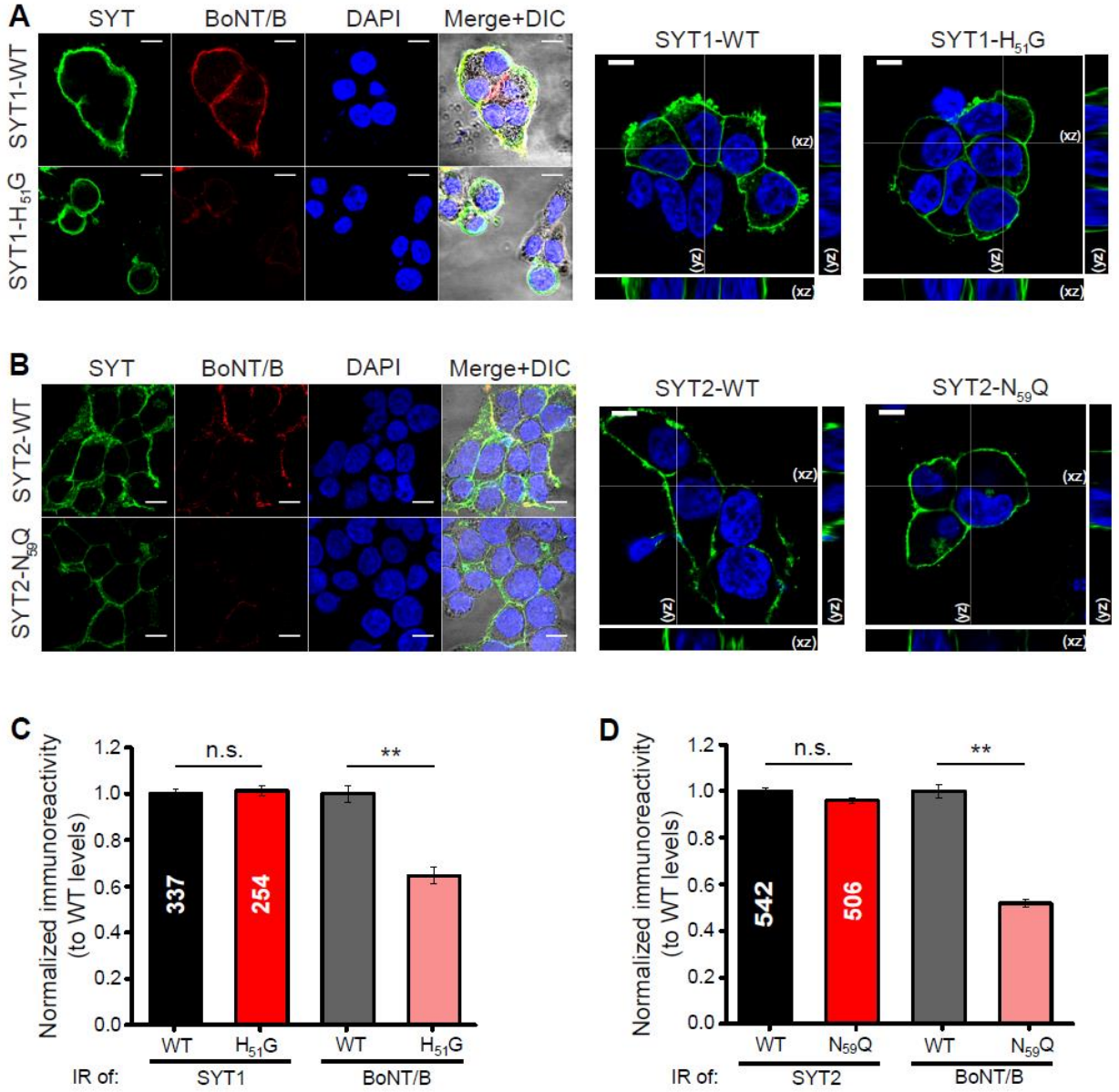

Fig. 7. **Mutations in the BoNT/B binding interface of SYTs decrease the binding of BoNT/B to HEK 293 cells.** (**A**) Immunostaining of SYT1 (green) and BoNT/B (red) in HEK 293 cells transfected with either SYT1-WT (top) or $H_{51}G$-SYT1 (bottom). DAPI signal is shown in blue, and the merge over DIC images indicated. Orthogonal projections of SYT1 labelling (green) in cells transfected with WT-SYT1 or SYT1-$H_{51}G$ (right). Scale bars, 10 µm. (**B**) Immunostaining of SYT2 (green) and BoNT/B (red) in HEK 293 cells transfected with either SYT2-WT (top panels) or SYT2-$N_{59}Q$ (bottom panels). DAPI signal is shown in blue, and the merge over DIC images indicated. Orthogonal projections of SYT2 labelling (green) in cells transfected with SYT2-WT or SYT2-$N_{59}Q$ (right). Scale bars, 10 µm. (**C**) Quantification of BoNT/B binding (grey and pink) and SYT1 expression (black and red) in cells expressing SYT1-WT or SYT1-$H_{51}G$. The number of ROIs analyzed is indicated within each column. Normalized immunoreactivity data (IR) are

expressed as mean ± SEM. Mann-Whitney U test was used for comparisons. **P < 0.01; n.s., non-significant. SYT1-WT IR to SYT1-H_{51}G IR P=0.64; BoNT/B SYT1-WT to BoNT/B SYT1-H_{51}G P=4.42 x 10^{-12}. (**D**) Quantification of BoNT/B binding (grey and pink) and SYT2 expression (black and red) in cells expressing SYT2-WT or SYT2-N_{59}Q. The number of ROIs analyzed is indicated within each column. Data are expressed as mean ± SEM. Mann-Whitney U test was used for comparisons. **P < 0.01; n.s., non-significant. SYT2-WT IR to SYT2-N_{59}Q IR P=0.64; BoNT/B SYT2-WT to BoNT/B SYT2-N_{59}Q P<0.001.